Geomechanical aspects of induced microseismicity during CO_2 injection in Illinois Basin

Nikita Bondarenko[1], Sherilyn Williams-Stroud[2], Jared Freiburg[2], and Roman Makhnenko[1]

https://doi.org/10.1190/tle40110823.1

Abstract

Carbon sequestration activities are increasing in a global effort to mitigate the effects of greenhouse gas emissions on the climate. Injection of wastewater and oil-field fluids is known to induce seismic activity. This makes it important to understand how that risk relates to CO_2 injection. Injection of supercritical CO_2 into the Cambrian Mt. Simon sandstone in Illinois Basin induced microseismicity that was observed below the reservoir, primarily in the Precambrian crystalline basement. Geomechanical and flow properties of rock samples from the involved formations were measured in the laboratory and compared with geophysical log data and petrographic analysis. The controlling factors for induced microseismicity in the basement seem to be the hydraulic connection between the reservoir and basement rock and reactivation of pre-existing faults or fractures in the basement. Additionally, the presence of a laterally continuous low-permeability layer between reservoir and basement may have prevented downward migration of pore pressure and reactivation of critically stressed planes of weakness in the basement. Results of the geomechanical characterization of this intermediate layer indicate that it may act as an effective barrier for fluid penetration into the basement and that induced microseismicity is likely to be controlled by the pre-existing system of faults. This is because the intact material is not expected to fail under the reservoir stress conditions.

Introduction

One of the mechanisms associated with induced seismic activity is the increase in reservoir pressures caused by commercial-scale underground fluid injection (Ellsworth, 2013). This is a major concern due to the potential for felt or damaging seismicity. However, it is believed that even small- to moderate-size earthquakes could threaten the seal integrity of CO_2 repositories (Zoback and Gorelick, 2012). Although induced microseismicity has been observed, earthquakes felt on the surface have not been reported for CO_2 injection sites (Vilarrasa et al., 2019). Sedimentary reservoirs targeted for CO_2 storage are rarely critically stressed. However, if the CO_2 injection pressure can migrate below the reservoir, it has the potential to reactivate pre-existing faults in the underlying crystalline basement that could be close to critical-stress states (Vilarrasa and Carrera, 2015). Crystalline basement rock should be put in focus because the majority of observed seismic events during underground fluid injection have occurred below the injection interval (Verdon, 2014). The permeability of typical intact crystalline rocks is lower than microdarcy (Jaeger et al., 2007). However, significant fluid migration is possible within the basement through fractures or faults, which can be up to four to five orders of magnitude more permeable than the intact material (Rutqvist, 2015). Pressure perturbation could reach large distances through the reservoir and reactivate optimally oriented distant faults (White and Foxall, 2016). An increase in the pore fluid pressure will lead to a decrease in the effective stress acting normal to fault surfaces. As a result, this brings the stress state closer to conditions associated with the slip along favorably oriented weak planes.

The presence of a low-permeable intermediate layer between reservoir and basement rock may prevent the downward migration of pressure perturbation into the basement. Monitoring of the Illinois Basin Decatur Project (IBDP) indicated that the induced microseismic events occurred primarily in the crystalline basement (Goertz-Allmann et al., 2017; Bauer et al., 2019). Additional analysis showed that many events are located in an area where seismic reflection data suggest a low-permeability intermediate layer between reservoir and basement is thin or missing (Williams-Stroud et al., 2020). This raises the question of which properties of the intermediate layer are responsible for reducing the number of microseismic events in the underlying formations. To address this question, thorough geomechanical characterization is conducted on the reservoir and basement material extracted from a wellbore drilled 25 km away from IBDP. Results of laboratory measurements are verified by comparison with log data from a wellbore at the injection site.

Geology and field observations

The target reservoir for CO_2 injection and storage in Illinois Basin is the lower unit of the Cambrian Mt. Simon sandstone. The injection zone at the Decatur site is close to the Precambrian rhyolite crystalline basement. Four deep wells drilled at the site (two injection and two monitoring wells) penetrate the top 20–30 m of the basement and suggest a rather complex volcanic terrain (Freiburg et al., 2020). The top veneer of this terrain and dominant lithology is rhyolite. Fractures are clearly visible in cores and image logs (Freiburg et al., 2020) and can be distinguished from drilling-induced fractures by minor diagenetic mineral alteration and cement along them.

At the IBDP site, the thickness of Mt. Simon sandstone is up to 500 m, with average porosity ϕ = 0.22 and permeability k = 200 mD (Freiburg et al., 2016). Between the Mt. Simon sandstone and the Precambrian rhyolite, a relatively thin (up to 30 m thick) Argenta unit unconformably overlies the basement. The unit dominantly consists of well-cemented quartz arenite with intervals of sandstone, conglomerate, siltstone, and mudstone and has a significantly lower porosity (ϕ = 0.09) and permeability (k = 2.3 mD) than Mt. Simon sandstone (Freiburg et al., 2014; Leetaru and Freiburg, 2014). Seismic reflection imaging suggests

[1]Department of Civil and Environmental Engineering, University of Illinois at Urbana-Champaign, Urbana, Illinois, USA. E-mail: nikitab3@illinois.edu; romanmax@illinois.edu.
[2]Illinois State Geological Survey, Champaign, Illinois, USA. E-mail: sherilyn@illinois.edu; freiburg@illinois.edu.

that the Argenta thins and is likely missing on Precambrian basement topographic highs, potentially providing a hydraulic connection with the reservoir (Williams-Stroud et al., 2020). In areas where the Argenta has sufficient thickness, it will likely restrict downward migration of the increased pore pressure and potentially prevent fault reactivation during CO_2 injection. However, the occurrence of induced seismicity during injection at the Decatur site confirms the existence of a hydraulic connection between the reservoir and pre-existing faults in the basement (Figure 1).

Industrial-scale CO_2 injection projects require multiple injection wells. One of the potential wells is the CarbonSAFE Christian County T. R. McMillen #2 well located approximately 25 km southwest of the IBDP site. The Precambrian basement in this well appears to be more homogeneous than that of IBDP but is similarly a rhyolite. In this well, fractures are also visible in the image logs (Figure 2) and in a few centimeter-scale X-ray computed tomography (CT) scans of the extracted cores of the rhyolite (Figure 3). Similar to the IBDP cores, minor diagenetic mineral alteration and cement along fractures specify a natural geologic origin as opposed to that induced by drilling. Comparison of geophysical logs for the T. R. McMillen #2 well with VW#1 at the IBDP site indicates that properties of the Precambrian rhyolite and Argenta sandstone are similar for these two locations. However, the crystalline basement at this location is about 220 m shallower than at IBDP, and seismic reflection data designate the presence of a topographic high west of the T. R. McMillen #2 well. Similar to the IBDP site, the thickness of the Argenta near the high may be insufficient to prevent the hydraulic connection between the reservoir and basement. This may induce observable microseismicity during CO_2 injection.

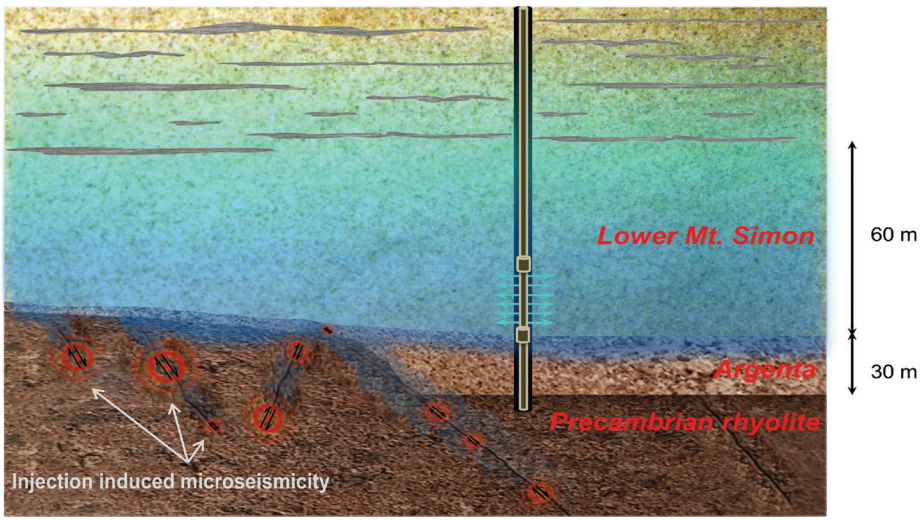

Figure 1. Sketch of possible pressure migration and fault reactivation in the Precambrian rhyolite due to the hydraulic connection between reservoir rock and pre-existing faults. Vertical flow of CO_2 to the upper part of the reservoir is restricted by low-permeability mudstone baffles, making flow dominantly horizontal.

Geomechanical and mineralogical characterization

Geomechanical characterization is conducted on cores of Argenta (extracted from depth between 1919 and 1920 m) and Precambrian rhyolite (extracted from depth between 1950 and 1970 m) from the T. R. McMillen #2 well in Christian County, Illinois. Laboratory testing includes petrographic analysis,

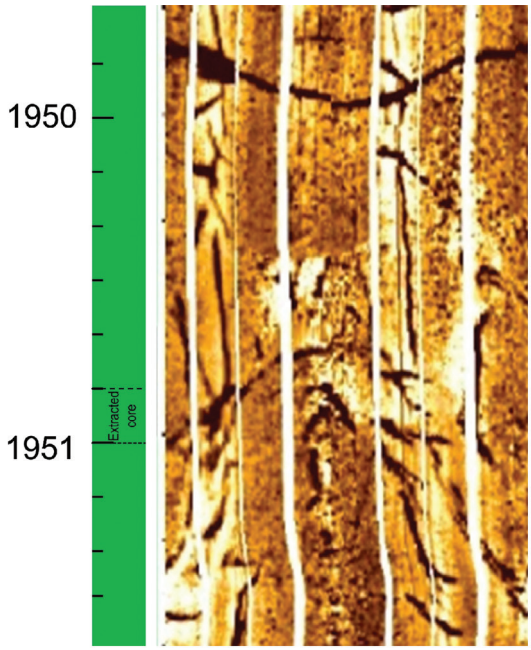

Figure 2. Image log from the T. R. McMillen #2 well showing fractures in the Precambrian rhyolite (depth is 1950 m).

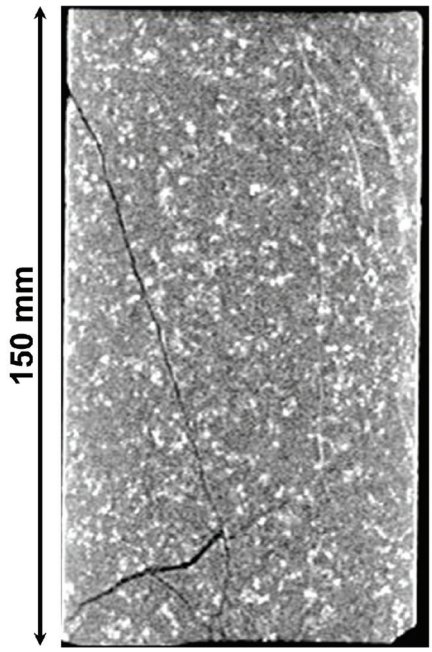

Figure 3. Sidewall projection X-ray CT scan of the Precambrian rhyolite specimen (depth is 1950 m) from the T. R. McMillen #2 well.

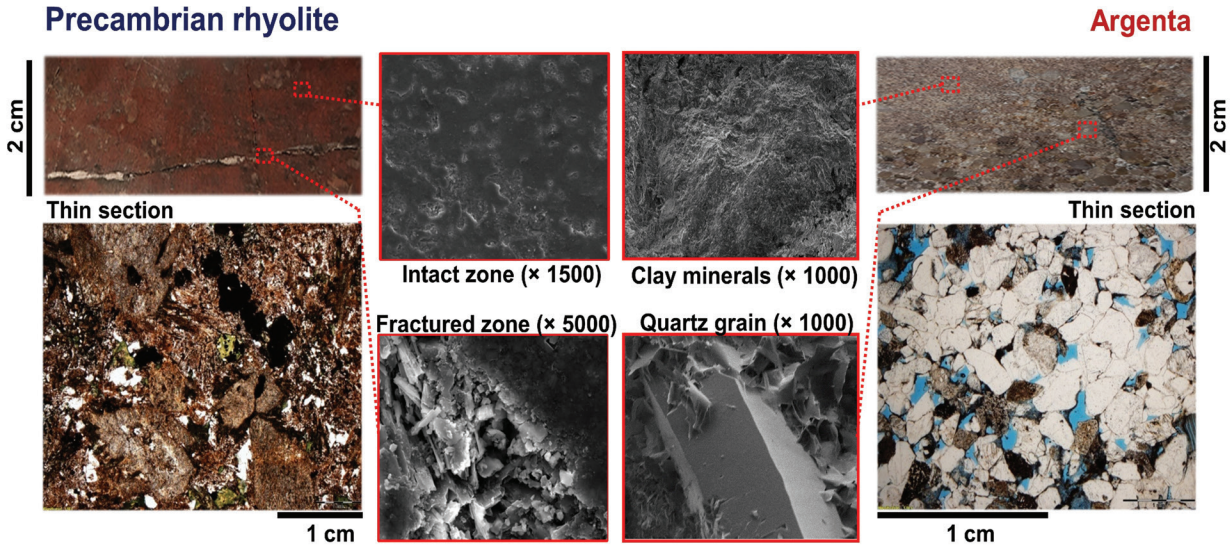

Figure 4. Core samples, scanning electron microscope photomicrographs, and thin-section photomicrographs of the Precambrian rhyolite and Argenta.

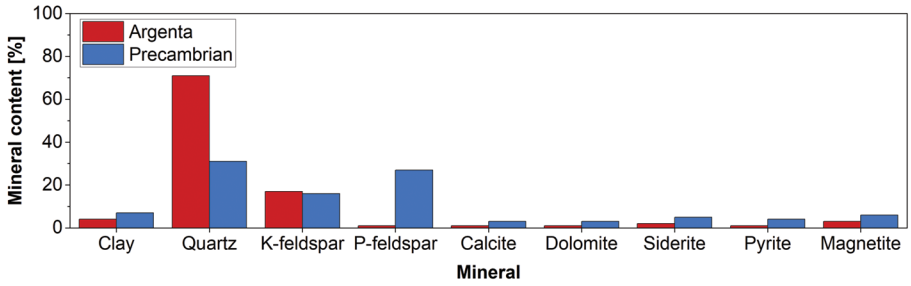

Figure 5. Mineral weight percent based on quantitative X-ray diffraction analysis of the Argenta (depth 1921 m) and Precambrian rhyolite (depth 1948 m) core samples from the T. R. McMillen #2 well.

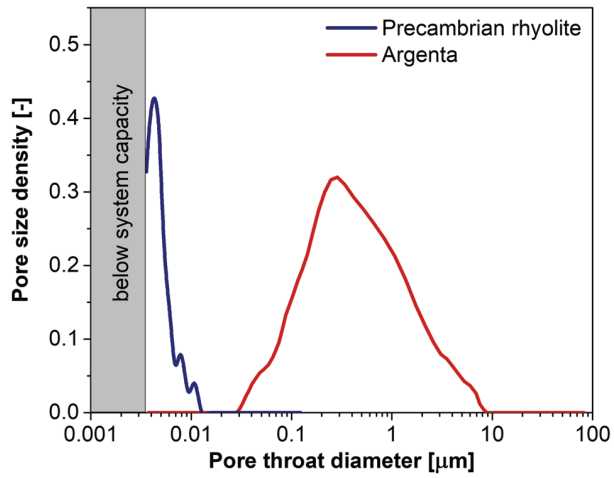

Figure 6. Pore-throat diameter distribution in the Precambrian rhyolite and Argenta samples from MIP. The dominant pore size is 0.005 µm for Precambrian rhyolite and 0.25 µm for Argenta.

porosimetry, measurements of ultrasonic velocities, permeability, elastic parameters, and strength characteristics of the involved formations.

The core samples used for geomechanical analysis consist of rhyolite for the crystalline basement and sandstone for the Argenta sample (Figure 4). A partially open fracture is observed in the basement core sample with some calcite cement and clay alteration along the fracture. The rhyolite dominantly consists of feldspar and quartz with minor clay and accessory minerals (Figure 5). It is porphyritic with feldspar phenocrysts and a finely crystalline felsic matrix. The Argenta sample is heterogeneous with interbedded layers of fine- and coarse-grained material (Figure 4). The sandstone is dominantly composed of quartz with minor K-feldspar, basement lithics, and clay. Detrital grains are subrounded with common authigenic quartz overgrowths cementing pore throats. Pore space is dominantly primary, with minor secondary porosity resulting from partial feldspar dissolution. Clays are common in pore space as well as grain and pore linings. Both authigenic clay and quartz cement are present in pore throats, isolating pore space and causing permeability of the sandstone to be relatively low.

Interconnected porosity and distribution of pore-throat diameters are accurately measured for both materials using mercury intrusion porosimetry (MIP). This method is based on precise volume measurements of intruded nonwetting fluid (mercury) with an increase of applied pressure (Ritter and Drake, 1945). The pore size for the Precambrian rhyolite sample is below 0.01 µm, with the dominant size of 0.004 µm. The interconnected porosity is measured to be ϕ = 0.5%. Due to the capacity of the system, the volume of pores smaller than 0.003 µm cannot be accessed; however, their contribution is expected to be significantly smaller than those of the dominant size. The presence of specimen-scale opened fractures may have a significant effect on porosity, which cannot be captured with the MIP. Therefore, the porosity of the Precambrian rhyolite with macroscopic fractures is expected to be higher. For the Argenta sample, the pore size ranges from 0.03 µm to tens of micrometers, with the dominant pore size of approximately 0.25 µm (Figure 6). The interconnected porosity is ϕ = 13.8%. Measured material properties for involved formations are summarized in Table 1.

Table 1. Summary of material properties for Argenta and Precambrian rhyolite formations.

Property	Argenta		Precambrian rhyolite	
	Lab data	Log data	Lab data	Log data
Dry bulk density, ρ_b (g/cm^3)	2.30	-	2.74	-
Dominant pore size, d (μm)	0.25	-	0.005	-
Porosity, ϕ (–)	0.138	0.12	0.005	0.03
P-wave velocity, c_p (km/s)	2.63	3.81	5.33	5.86
S-wave velocity, c_s (km/s)	1.61	2.09	3.28	3.39
Dynamic Young's modulus, E_d (GPa)	14.3	27.2	71.1	80.9
Dynamic Poisson's ratio, ν_d (–)	0.19	0.28	0.20	0.25
Static Young's modulus, E (GPa)	10.7	-	52.0	-
Static Poisson's ratio, ν (–)	0.22	-	0.22	-
Uniaxial compression strength, UCS (MPa)	44	-	189	-
Cohesion, c (MPa)	9.5	-	0*	-
Friction angle, φ (°)	45	-	61	-
Permeability, k (μD)	5.3	10^3	0.7×10^{-3} – intact[1] about $1–10^3$ – fractured	< 10

*The cohesion on a weak plane in Precambrian rhyolite is close to zero.
[1]Indirect estimation from Makhnenko et al. (2020).

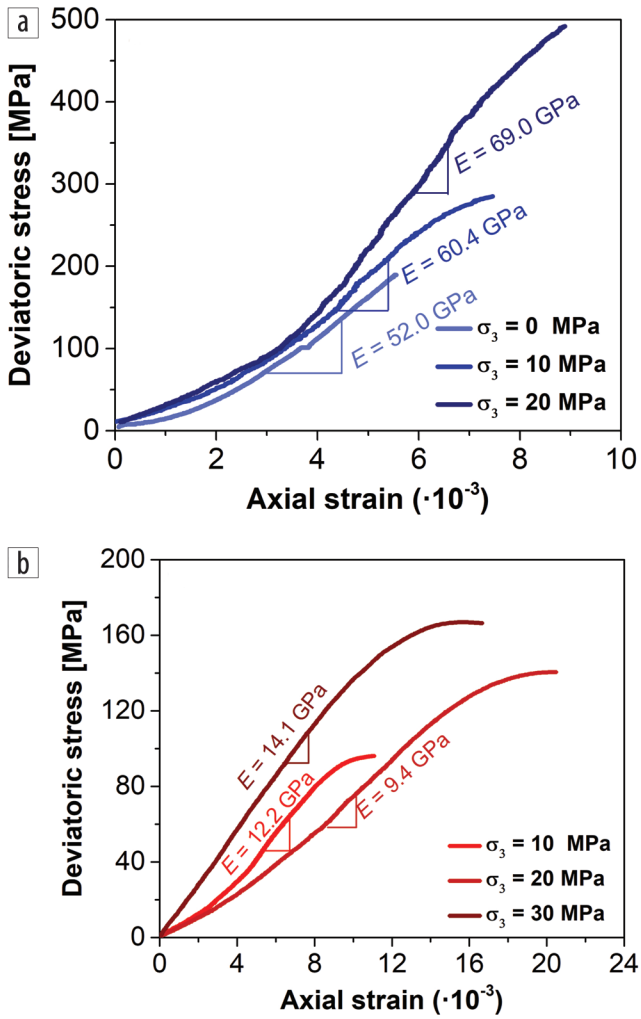

Figure 7. Results of conventional triaxial tests on (a) Precambrian rhyolite and (b) Argenta specimens.

Ultrasonic or "dynamic" elastic properties are calculated from the measurements of wave velocities and bulk density (Brown, 1981). The tests are conducted in the lab on dry unconfined rock cores with sets of 2.25 MHz P- and S-wave transducers. The couplant is placed between the transducer and sample surface to improve wave transmission efficiency. Signal-to-noise ratio was improved by time averaging of 128 recorded waveforms. The departure and arrival times for P- and S-waves are determined by visual and digital analysis of the waveforms to calculate compressional and shear-wave velocities c_p and c_s. After measurements of the material bulk density ρ_b, the dynamic Young's modulus E_d and dynamic Poisson's ratio ν_d can be calculated. Results of ultrasonic velocity measurements for the Precambrian rhyolite and Argenta sandstone and comparison with geophysical well-log data are shown in Table 1.

A series of uniaxial and conventional triaxial tests was conducted using a 1 MN MTS load frame with a Hoek-Franklin triaxial cell. During the tests, the specimen's deformation is measured with strain gages (uniaxial test) or calculated from axial displacement corrected for machine stiffness (triaxial test). The specimens are cored in the direction perpendicular to the core axis. The measured response of Precambrian rhyolite (Figure 7a) and Argenta sandstone (Figure 7b) at different values of minor principal stress σ_3 is used to evaluate the strength and elastic properties of the involved formations. Measured Poisson's ratio at σ_3 = 0 MPa is 0.22 for both Precambrian rhyolite and Argenta. The material's response is nonlinear at the early stages of loading, indicating the presence of cracks and crack-like pores in the tested formations. Measured Young's modulus E increases with the applied minor principal stress σ_3. It ranges from 52 to 69 GPa for Precambrian rhyolite at σ_3 = 0–20 MPa. The Young's modulus of Argenta is between 9.4 and 14.1 GPa for σ_3 = 0–40 MPa.

Results of the conventional triaxial tests are interpreted within the framework of the Mohr-Coulomb failure criterion (Labuz and Zang, 2012) to obtain the strength characteristics: cohesion c and friction angle φ (Figure 8). The cohesion is calculated to be 22.0 and 9.5 MPa for Precambrian rhyolite and Argenta, respectively. The friction angle at low effective mean stress is calculated to be 61° for Precambrian rhyolite and 42° for Argenta sandstone, which seems to be slightly larger than typical values for these types of rock reported in the literature (Jaeger et al., 2007; Labuz et al., 2018). However, the triaxial compression test conducted on Argenta specimens at confining pressures of σ_3 = 30 and 40 MPa indicated that at higher effective mean stress values, failure envelope becomes nonlinear and lower friction angle is expected. In addition, all of the apparently intact Precambrian rhyolite specimens failed through pre-existing weak planes that were not visible during specimen preparation. Numerous attempts to prepare specimens of Precambrian rhyolite with visible cemented fractures resulted in

the creation of open fractures and specimen failure. Therefore, it is assumed that the cohesion of the specimens with visible weak planes is small, and the failure envelope for Precambrian rhyolite in Figure 8 is shifted to zero cohesion. The friction angle for visible sealed fractures would depend on the filling material and may be significantly lower than that for the material without sealed fractures.

Intrinsic permeability k, a parameter that governs steady fluid flow due to pressure gradient, is widely used to represent hydraulic behavior. This parameter only depends on the characteristics of the material and is independent of fluid properties. Permeability of the Precambrian rhyolite specimen with open fracture oriented subparallel to the flow direction and the intact Argenta sandstone specimen was measured with the steady-state flow method (Boulin et al., 2012). The permeability of the Argenta is on the order of microdarcy and is stress dependent (ranges from 5.3 to 1.4 μD for effective mean stress between 2 and 25 MPa). The permeability of intact Precambrian rhyolite is estimated from a transient method to be approximately 1 nD (Makhnenko et al., 2020). The measured permeability of the Precambrian rhyolite specimen with an open fracture is in the microdarcy range, significantly decreasing with applied mean stress. At the same time, the permeability of the fractured basement rock was found to be strongly dependent on specimen setup, which affected fracture orientation and aperture (measured permeability could reach tens of millidarcy if the fracture offset is large). Along with the contrast between permeability of intact and fractured material, this highlights the role of fractures and the necessity of addressing their effect on hydraulic and mechanical properties of the rock. Measured values and comparison with log data are reported in Table 1.

Discussion

Laboratory geomechanical testing enables the conduction of accurate direct measurements of the material properties at controlled experimental conditions. However, laboratory experiments are limited to specimens of linear dimensions only up to a few centimeters. On the other hand, geophysical wellbore log data provide data on the field scale, though the mechanical properties are derived from ultrasonic logs and not measured directly. Therefore, comparison and verification of the data from both sources is important.

Measurement of ultrasonic and sonic velocities is a widely used technique in the laboratory and in geophysical well logging, where it is utilized to characterize the dynamic elastic properties of rock formations. According to the data reported in Table 1, ultrasonic velocities measured in the laboratory are lower compared to the log data, resulting in lab dynamic elastic properties being lower than those from the field. One possible explanation is that laboratory measurements are conducted on unconfined dry specimens, which are not representative of in-situ conditions. In nature, high mean stress will cause partial closure of pre-existing crack-like pores, and elastic waves could propagate faster (Yukutake et al., 1988; Mavko et al., 2009; Schmitt, 2015). Another critical aspect during measurements is fluid saturation of cores. In-situ rocks at depths of several kilometers are usually fluid saturated with aqueous fluids, and it could make the measured velocities for dry and fluid-saturated cores significantly different (Johnston and Toksöz, 1980; Cristensen and Wang, 1985; Makhnenko et al., 2020).

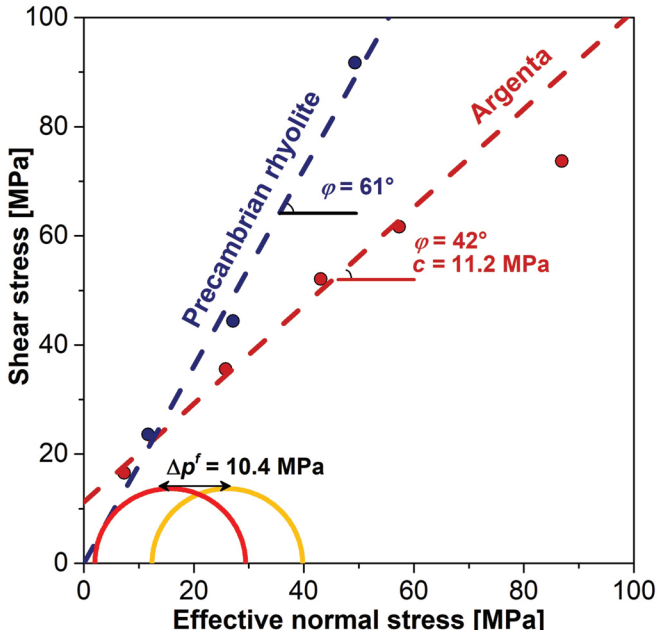

Figure 8. Mohr-Coulomb failure envelope for basement rock (shifted to accommodate the assumption of zero cohesion on a visible pre-existing weak plane) and Argenta. The orange Mohr's circle represents the effective stress state at the top of the basement rock layer in Illinois Basin estimated from Bauer et al. (2016). The red Mohr's circle represents the potential stress state at failure. Details on stress state are provided in the discussion section.

Therefore, laboratory measurements of ultrasonic velocities on unconfined dry specimens may underestimate dynamic elastic properties, and measurements should be conducted at the conditions representative to the in situ in terms of applied mean stress, fluid saturation, pore pressure, etc.

Another critical aspect is understanding the difference between dynamic and static elastic properties. Dynamic elastic properties represent the material response to high-frequency loading (e.g., wave propagation created by an earthquake), while static properties represent the material response to quasi-static loading (e.g., that applied by a load frame in a conventional triaxial compression test). Dynamic properties are usually significantly larger compared to static (Brotons et al., 2016), and empirical correlations are utilized for the estimation of static moduli from ultrasonic log data (Fjar et al., 2008). However, laboratory experiments enable assessing them directly during conventional triaxial tests at representative conditions and capturing stress dependency of the material elastic properties. These properties should be utilized for numerical modeling of the quasi-static process of CO_2 injection using the proper upscaling approaches (Lei et al., 2015).

Possible upper and lower boundaries of elastic properties may be estimated using the effective media approach for known mineral composition and elastic moduli of the minerals, which constitute the rock matrix and can be adopted from the literature (Mavko et al., 2009). The most conservative relationship for the lower and upper boundaries is found in Reuss (1929) and Voigt (1889), respectively. The simple arithmetic average between the upper and lower boundaries (Voigt-Reuss-Hill estimation) for Young's modulus and Poisson's ratio is shown in Figure 9 and compared to the values obtained from the laboratory and log measurements.

Permeability appears to be the most sensitive material property to the measurements performed in the field and lab (Table 1). Estimation of permeability from log data is based on inversion of porosity measurements. However, the appropriate permeability model should be selected based on fluid composition and data from geologic and petrophysical analysis (Ahmed et al., 1991; Fjar et al., 2008). Permeability estimates from geophysical logs in the Argenta sandstone are on the order of millidarcy, while laboratory measurement results are on the order of microdarcy. This huge gap is likely to be related to the differences between laboratory and field scales. Laboratory specimens are usually intact and do not contain large or open fractures. At the field scale, large regions composed of low-permeability rocks are often significantly more permeable than small volumes of the same rock due to the presence of joints, fractures, and faults (Neuzil, 1986). Properties of the specimens with fractures may be measured in the laboratory; however, upscaling to the reservoir scale is nontrivial (e.g., Lei et al., 2015). On the other hand, laboratory experiments provide robust data for the intact material at conditions representative of the in situ and provide constraints for log permeability models at discrete locations in the wellbore (Kim and Makhnenko, 2020). Therefore, it seems reasonable to assume that results of geophysical measurements represent averaged permeability of material with fractures, while results of laboratory measurements characterize permeability of the intact material, unless the permeability of fractures is purposefully measured.

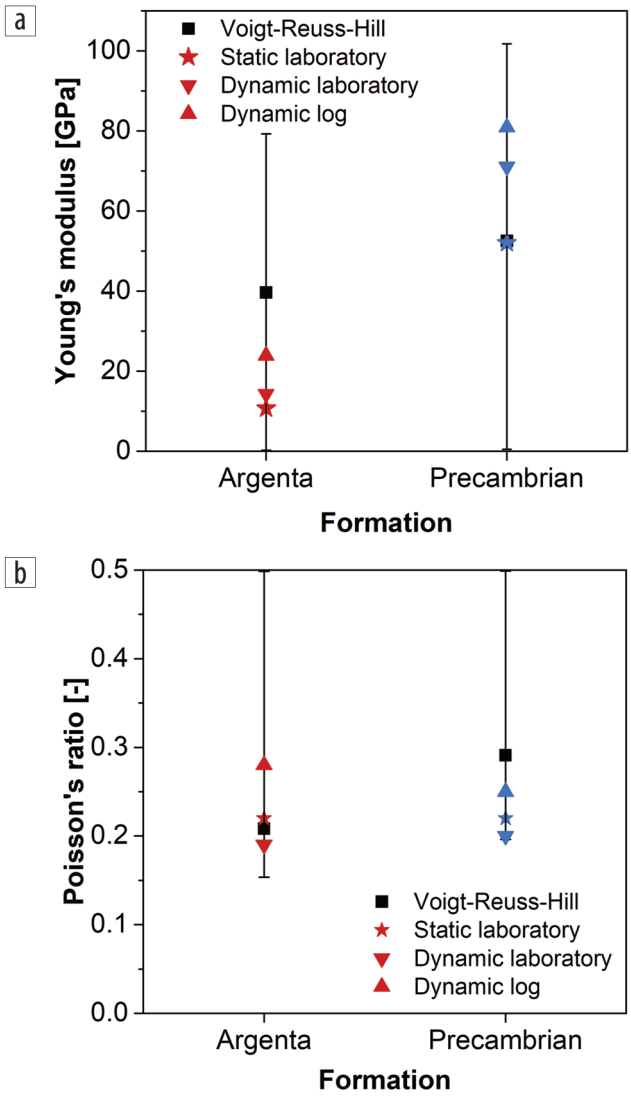

Figure 9. Comparison between the dynamic, static, and log measurements of (a) Young's modulus and (b) Poisson's ratio and estimation from the effective media theory.

Using averaged permeability of fractured material based on geophysical measurements is qualitatively similar to the approach of equivalent porous media in which the presence of fractures is captured implicitly through reduction of material properties instead of direct consideration of fractures. Some numerical investigations have shown that pressure distribution in the reservoir and fracture stability are not well captured with the equivalent medium but requires explicit inclusion of the fractures in the model (Zareidarmiyan et al., 2021). Due to the complexity of the experiments with the fractured rock, the number of previous studies is limited, even though material-specific stress-dependent fracture permeability and the effect of fracture surface roughness have been reported (Li et al., 2021). The type of pore fluid and CO_2 injection conditions can also influence the frictional strength and fault reactivation in the geomaterials over long timescales (Samuelson and Spiers, 2012; Vilarrasa et al., 2019). This may be insignificant for Argenta or Precambrian rhyolite because the CO_2 plume would not be expected to reach the basement rock due to buoyancy. Therefore, evaluation of induced seismicity potential in the crystalline basement in the short term should be more focused on assessment of fluid overpressure transfer in fractured media rather than interaction between crystalline basement and CO_2. However, in the long term, CO_2 may reach underlying layers due to the presence of layers that inhibit upward migration. Geophysical field measurements can be missing the important features of the fluid-rock interaction. Therefore, the laboratory investigation of fractured rock response could be essential despite the complexity of these experiments.

Geophysical log data and geomechanical laboratory data estimate the average permeability of the Argenta layer between reservoir and basement rock to be 10^3 and a few microdarcy, respectively. The significantly lower permeability of the Argenta compared to the Mt. Simon sandstone (average 200 mD) indicates that it will inhibit downward migration of the excessive pore pressure created by CO_2 injection. If the Argenta layer is missing or if pressure could be transmitted into the basement through high-permeability faults, conditions for triggering slip along a favorably oriented pre-existing fault in the basement could develop. The Argenta is interpreted as a shallow marine deposit that onlaps and thins or is missing on Precambrian topographic highs in the Illinois Basin (Freiburg et al., 2014). Within the basin interior, the Argenta thickens significantly, thus a Mt. Simon reservoir and Precambrian interface is unlikely. On the shoulders of the basin where this interface is likely, injection near the base of the Mt. Simon Formation may increase the potential for hydraulic connection to the basement. However, the induced seismicity at the IBDP site indicates that these small "windows" into the basement are also possible in more interior basin locations. Reservoir models calibrated with CO_2 injection data showed that low-permeability lenses within the Mt.

Simon Formation (shown in Figure 1) had a significant impact on pressure and CO_2 migration, making it dominantly horizontal (Senel et al., 2014). Injection below these flow baffles near a zone with hydraulic communication to the basement likely caused the observed seismicity at the Decatur site. At the same time, the injection in the second well at the site into a zone that is a few tens of meters shallower has been followed by a significantly reduced seismicity rate, similar to that observed nearly two years after injection stopped in the first well (Williams-Stroud et al., 2020).

Induced microseismicity at IBDP is believed to be controlled by the presence of pre-existing weak planes in the Precambrian rhyolite and Argenta rather than failure of intact material. Geomechanical characterization indicated that crystalline basement contains weak pre-existing fractures. This is also confirmed by results of laboratory strength measurements (Figure 8). The minor principal total stress at the injection site is horizontal and measured with the injection and step rate tests as $\sigma_h = \sigma_3 = 34.2$ MPa. The vertical stress is estimated from the integrated density method as $\sigma_V = \sigma_2 = 50.8$ MPa. The major principal stress is horizontal and calculated to be $\sigma_H = \sigma_1 = 61.6$ MPa based on geomechanical modeling with a ratio of $\sigma_H/\sigma_h = 1.8$. The pore pressure $p^f = 21.8$ MPa is slightly above the hydrostatic value. The first motion analysis of the induced events indicates strike-slip failure, consistent with the major and minor principal stresses calculated as being horizontal (Bauer et al., 2016). The Mohr's circle shown in Figure 8 corresponds to the original state of the effective stress at the injection well at the top of the Precambrian rhyolite in Illinois Basin. The necessary change of pore pressure to cause failure of the basement rock is approximately 10.4 MPa, assuming that the failure occurs through a cohesionless joint that has the same friction angle as the tested specimens. This pressure is far above the maximum increase in the pore pressure (approximately 1.2 MPa) recorded in the reservoir during the injection phase at IBDP (Bauer et al., 2016). Consequently, the observed induced microseismicity is likely to be associated with reactivation of favorably oriented weak planes, where friction angle may be lower due to the presence of infilling material, or incomplete cement bridges in fractures. At the same time, the strength of Precambrian rhyolite was estimated based on laboratory experiments performed on specimens without visible cracks and may be an overestimation for the fractured material. More accurate evaluation of induced seismicity potential would require thorough strength measurements on the basement rock specimens with visible fractures, which should involve purposefully designed preparation and experimental procedures.

Conclusions and perspectives

This study is focused on the geomechanical characterization of formations involved in induced microseismicity during CO_2 injection in Illinois Basin. Data from micro, laboratory, and field scales are compiled and compared to determine which geomechanical properties are responsible for the observed microseismic activity. The crystalline basement consisting of Precambrian rhyolite appears to contain weak planes, which may be close to critical-stress state and reactivated by the excess pore pressure caused by CO_2 injection. Intact Precambrian rhyolite has very low permeability; however, hydraulic connection between the reservoir and basement may be provided through high-permeability fractures, as well as through direct contact between the basement and reservoir away from the injection location. An intermediate layer (Argenta) between the reservoir and basement rock is at least three orders of magnitude less permeable than the reservoir. It restricts the downward migration of pore pressure disturbance and, as a result, can also prevent reactivation of pre-existing faults in the basement. An intermediate layer of sufficient thickness is an effective seal for the basement, and confirmation of the presence of this layer should be an important component of site assessments for potential CO_2 injection. Strength tests performed on the Precambrian rhyolite and Argenta sandstone indicate that failure of intact material requires very high overpressure and is unlikely to occur. In areas where seismic reflection data quality makes it difficult prior to injection to identify faults and fractures susceptible to reactivation, or where confirmation of a low-permeability barrier to the basement is not possible, an assessment of the likelihood of induced microearthquakes can be supported by the investigation of the potential impact of the pre-existing fractures on the material response due to CO_2 injection. TLE

Acknowledgments

The authors acknowledge support from the U.S. Department of Energy through the CarbonSAFE Macon County Project DE-FE0029381. They also thank the editors, V. Vilarrasa, and an anonymous reviewer for detailed comments that helped improve the quality of the manuscript.

Data and materials availability

Data associated with this research are available and can be obtained by contacting the corresponding author.

Corresponding author: nikitab3@illinois.edu

References

Ahmed, U., S. F. Crary, and G. R. Coates, 1991, Permeability estimation: The various sources and their interrelationships: Journal of Petroleum Technology, **43**, no. 5, 578–587, https://doi.org/10.2118/19604-PA.

Bauer, R. A., R. Will, S. Greenberg, and S. G. Whittaker, 2019, Illinois Basin-Decatur Project, *in* T. L. Davis, M. Landrø, and M. Wilson, eds., Geophysics and geosequestration: Cambridge University Press, 339–369, https://doi.org/10.1017/9781316480724.020.

Bauer, R. A., M. Carney, and R. J. Finley, 2016, Overview of microseismic response to CO_2 injection into the Mt. Simon saline reservoir at the Illinois Basin-Decatur Project: International Journal of Greenhouse Gas Control, **54**, no. 1, 378–388, https://doi.org/10.1016/j.ijggc.2015.12.015.

Boulin, P. F., P. Bretonnier, N. Gland, and J. M. Lombard, 2012, Contribution of the steady state method to water permeability measurement in very low permeability porous media: Oil and Gas Science and Technology – Revue d'IFP Energies nouvelles, **67**, no. 3, 387–401, https://doi.org/10.2516/ogst/2011169.

Brotons, V., R. Tomás, S. Ivorra, S. Grediaga, J. Martínez- Martínez, D. Benavente, and M. Gómez-Heras, 2016, Improved correlation between the static and dynamic elastic modulus of different types of rocks: Materials and Structures, **49**, 3021–3037, https://doi.org/10.1617/s11527-015-0702-7.

Brown, E. T., 1981, Rock characterization, testing and monitoring: ISRM suggested methods: Pergamon Press.

Christensen, N. I., and H. F. Wang, 1985, The influence of pore pressure and confining pressure on dynamic elastic properties of Berea sandstone: Geophysics, **50**, no. 2, 207–213, https://doi.org/10.1190/1.1441910.

Ellsworth, W. L, 2013, Injection-induced earthquakes: Science, **341**, no. 6142, https://doi.org/10.1126/science.1225942.

Fjær, E., R. Holt, P. Horsrud, and A. Raaen, 2008, Petroleum related rock mechanics: Elsevier.

Freiburg, J. T., J. H. McBride, D. H. Malone, and H. E. Leetaru, 2020, Petrology, geochronology, and geophysical characterization of Mesoproterozoic rocks in central Illinois, USA: Geoscience Frontiers, **11**, no. 2, 581–596, https://doi.org/10.1016/j.gsf.2019.07.004.

Freiburg, J. T., R. W. Ritzi, and K. S. Kehoe, 2016, Depositional and diagenetic controls on anomalously high porosity within a deeply buried CO_2 storage reservoir — The Cambrian Mt. Simon sandstone, Illinois Basin, USA: International Journal of Greenhouse Gas Control, **55**, 42–54, https://doi.org/10.1016/j.ijggc.2016.11.005.

Freiburg, J. T., D. G. Morse, H. E. Leetaru, R. P. Hoss, and Q. Yan, 2014, A depositional and diagenetic characterization of the Mt. Simon sandstone at the Illinois Basin-Decatur Project carbon capture and storage site, Decatur, Illinois, USA: Illinois State Geological Survey.

Goertz-Allmann, B. P., S. J. Gibbons, V. Oye, R. Bauer, and R. Will, 2017, Characterization of induced seismicity patterns derived from internal structure in event clusters: Journal of Geophysical Research: Solid Earth, **122**, no. 5, 3875–3894, https://doi.org/10.1002/2016JB013731.

Jaeger, J. C., N. G. W. Cook, and R. Zimmerman, 2007, Fundamentals of rock mechanics, fourth edition: Wiley-Blackwell.

Johnston, D. H., and M. N. Toksöz, 1980, Ultrasonic P and S wave attenuation in dry and saturated rocks under pressure: Journal of Geophysical Research: Solid Earth, **85**, no. B2, 925–936, https://doi.org/10.1029/JB085iB02p00925.

Kim, K., and R. Y. Makhnenko, 2020, Coupling between poromechanical behavior and fluid flow in tight rock: Transport in Porous Media, **135**, 487–512, https://doi.org/10.1007/s11242-020-01484-z.

Labuz, J. F., and A. Zang, 2012, Mohr-Coulomb failure criterion: Rock Mechanics and Rock Engineering, **45**, 975–979, https://doi.org/10.1007/s00603-012-0281-7.

Labuz, J. F., F. Zeng, R. Makhnenko, and Y. Li, 2018, Brittle failure of rock: A review and general linear criterion: Journal of Structural Geology, **112**, 7–28, https://doi.org/10.1016/j.jsg.2018.04.007.

Leetaru, H. E., and J. T. Freiburg, 2014, Litho-facies and reservoir characterization of the Mt. Simon sandstone at the Illinois Basin — Decatur Project: Greenhouse Gases: Science and Technology, **4**, no. 5, 580–595, https://doi.org/10.1002/ghg.1453.

Lei, Q., J. P. Latham, C.-F. Tsang, J. Xiang, and P. Lang, 2015, A new approach to upscaling fracture network models while preserving geostatistical and geomechanical characteristics: Journal of Geophysical Research: Solid Earth, **120**, no. 7, 4784–4807, https://doi.org/10.1002/2014JB011736.

Li, W., L. P. Frash, N. J. Welch, J. W. Carey, M. Meng, and M. Wigand, 2021, Stress-dependent fracture permeability measurements and implications for shale gas production: Fuel, **290**, https://doi.org/10.1016/j.fuel.2020.119984.

Makhnenko, R. Y., C. Ge, and J. F. Labuz, 2020, Localization of deformation in fluid-saturated rock: International Journal of Rock Mechanics and Mining Sciences, **134**, https://doi.org/10.1016/j.ijrmms.2020.104455.

Makhnenko, R. Y., N. B. Bondarenko, K. Kim, and S. Whittaker, 2020, Laboratory modeling of induced microseismicity in the Illinois Basin: Presented at the 54th U.S. Rock Mechanics/Geomechanics Symposium.

Mavko, G., T. Mukerji, and J. Dvorkin, 2009, The rock physics handbook: Tools for seismic analysis of porous media: Cambridge University Press.

Neuzil, C. E., 1986, Groundwater flow in low-permeability environments: Water Resources Research, **22**, no. 8, 1163–1195, https://doi.org/10.1029/WR022i008p01163.

Reuss, A., 1929, Berechnung der fließgrenze von mischkristallen auf grund der plastizitätsbedingung für einkristalle: Zeitschrift für Angewandte Mathematik und Mechanik, **9**, no. 1, 49–58, https://doi.org/10.1002/zamm.19290090104.

Ritter, H. L. and L. C. Drake, 1945, Pore-size distribution in porous materials: Pressure porosimeter and determination of complete macropore-size distributions: Industrial and Engineering Chemistry, Analytical Edition, **17**, no. 12, 782–786, https://doi.org/10.1021/i560148a013.

Rutqvist, J., 2015, Fractured rock stress-permeability relationships from in situ data and effects of temperature and chemical-mechanical couplings: Geofluids, **15**, no. 1–2, 48–66, https://doi.org/10.1111/gfl.12089.

Samuelson, J., and C. J. Spiers, 2012, Fault friction and slip stability not affected by CO_2 storage: Evidence from short-term laboratory experiments on North Sea reservoir sandstones and caprocks: International Journal of Greenhouse Gas Control, **11**, S78–S90, https://doi.org/10.1016/j.ijggc.2012.09.018.

Schmitt, D. R., 2015, Geophysical properties of the near surface earth: Seismic properties, *in* G. Schubert, ed., Treatise on geophysics: Elsevier, 43–87, https://doi.org/10.1016/B978-0-444-53802-4.00190-1.

Senel, O., R. Will, and R. J. Butsch, 2014, Integrated reservoir modeling at the Illinois Basin — Decatur Project: Greenhouse Gases: Science and Technology, **4**, no. 5, 662–684, https://doi.org/10.1002/ghg.1451.

Verdon, J., 2014, Significance for secure CO_2 storage of earthquakes induced by fluid injection: Environmental Research Letters, **9**, no. 6, https://doi.org/10.1088/1748-9326/9/6/064022.

Vilarrasa, V., and J. Carrera, 2015, Geologic carbon storage is unlikely to trigger large earthquakes and reactivate faults through which CO_2 could leak: Proceedings of the National Academy of Sciences USA, **112**, no. 19, 5938–5943, https://doi.org/10.1073/pnas.1413284112.

Vilarrasa, V., R. Y. Makhnenko, and J. Rutqvist, 2019, Chapter 9: Field and laboratory studies of geomechanical response to the injection of CO_2, *in* P. Newell and A. Ilgen, eds., Science of carbon storage in deep saline formations: Process coupling across time and spatial scales: Elsevier, 209–236, https://doi.org/10.1016/B978-0-12-812752-0.00009-5.

Voigt, W., 1889, Ueber die Beziehung zwischen den beiden Elasticitätsconstanten isotroper Körper: Annalen der Physik, **274**, no. 12, 573–587, https://doi.org/10.1002/andp.18892741206.

White, J. A., and W. Foxall, 2016, Assessing induced seismicity risk at CO_2 storage projects: Recent progress and remaining challenges: International Journal of Greenhouse Gas Control, **49**, 413–434, https://doi.org/10.1016/j.ijggc.2016.03.021.

Williams-Stroud, S., R. Bauer, H. Leetaru, V. Oye, F. Stanek, S. Greenberg, and N. Langet, 2020, Analysis of microseismicity and reactivated fault size to assess the potential for felt events by CO_2 injection in the Illinois Basin: Bulletin of the Seismological Society of America, **110**, no. 5, 2188–2204, https://doi.org/10.1785/0120200112.

Yukutake, H., T. Nakajima, and K. Doi, 1988, In situ measurements of elastic wave velocity in a mine, and the effects of water and stress on their variation: Tectonophysics, **149**, no. 1–2, 165–175, https://doi.org/10.1016/0040-1951(88)90124-2.

Zareidarmiyan, A., F. Parisio, R. Y. Makhnenko, H. Salarirad, and V. Vilarrasa, 2021, How equivalent are equivalent porous media?: Geophysical Research Letters, **48**, no. 9, https://doi.org/10.1029/2020GL089163.

Zoback, M. D., and S. M. Gorelick, 2012, Earthquake triggering and large-scale geologic storage of carbon dioxide: Proceedings of the National Academy of Sciences of the United States of America, **109**, no. 26, 10164–10168, https://doi.org/10.1073/pnas.1202473109.